Lipid-Core/Polymer-Shell Hybrid Nanoparticles: Synthesis and Characterization by Fluorescence Labeling and Electrophoresis

Sophie Bou, Xinyue Wang, Nicolas Anton, Redouane Bouchaala, Andrey S Klymchenko, Mayeul Collot

ARTICLE

Lipid-Core/Polymer-Shell Hybrid Nanoparticles: Synthesis and Characterization by Fluorescence Labeling and Electrophoresis

Received 00th January 20xx,
Accepted 00th January 20xx

DOI: 10.1039/x0xx00000x

Sophie Bou,[1] Xinyue Wang,[2] Nicolas Anton,[2] Redouane Bouchaala,[1] Andrey S. Klymchenko,[1] Mayeul Collot[1*]

Among the lipid nanoparticles, Lipid Polymer Hybrid Nanoparticles (HNPs) composed of an oily core and a polymeric shell, display interesting features as efficient drug carriers due to the high loading capability of the oil phase and the stability and surface functionalization of the polymer shell. Herein, we formulated lipid-core/polymer-shell hybrid nanoparticles (HNPs) by a simple nanoprecipitation method involving Vitamin E Acetate (VEA) as the oily core and a tailor-made amphiphilic polymer as a wrapping shell. The fluorescence labeling of the oil, using a newly developed green fluorogenic BODIPY tracker, and of the polymer using a covalent attachment of a red emitting rhodamine allowed to assessing the formation, the composition and the stability of these new hybrid nanoparticles using dual color electrophoresis gel analysis. This technique, combined to conventional DLS and electronic microscopy analysis, allowed us to quickly determine that 20 wt % of polymer was an optimal ratio for obtaining stable HNPs by nanoprecipiation. Finally, we showed that using different polymeric shells, various HNPs can be obtained and finely discriminated by combined electrophoresis and two-color labeling approach.

1. Introduction

In the field of nanomaterials, lipid-based nanoparticles are drawing a growing interest especially as promising drug delivery systems, mainly due to the huge possibilities of lipophilic molecule loading they offer.[1,2] Among these nanoparticles, NanoEmulsions (NEs),[3, 4, 5] Solid Lipid Nanoparticles (SLNs) [6, 7, 8] and Nanostructured Lipid Carriers (NLCs)[9, 10] are composed of a lipid core that can serve as an efficient carrier of hydrophobic cargo such as drugs or contrast agents. Those lipid NPs are usually stabilized by monomeric surfactant or natural phospholipids with reduced possibilities of chemical modification thus limiting the modification of their physico-chemical properties, their biodistribution, their circulation time in blood[11, 12] or their targeting ability. Conversely, Polymeric Nanoparticles (PNPs) offer a wide diversity in their structures and functions due to accessible chemical modifications.[13, 14, 15, 16, 17] Consequently Lipid Polymer Hybrid Nanoparticles (HNPs) featuring the advantages of flexibility in the polymer design constitute promising new nanomaterials.[18] It is noteworthy that while polymeric core-lipid shell HNPs were extensively described,[19 20, 21, 22] those merging the advantage of an oily core with a polymeric shell, also called nanocapsules, remains poorly reported.[23, 24, 25] Therefore, a better comprehension on their formation and stability is required along with adapted analysis and characterization methods. Fluorescent labeling of lipid-based nanoparticles was used for bioimaging,[26, 27] and for *in cellulo*[28] and *in vivo*[29] tracking of single particles. Additionally, it is also an efficient method of characterization using various fluorescence techniques including microscopy[29] and fluorescence correlation spectroscopy.[28, 30] Although HNPs are generally characterized by dynamic light scattering (DLS) and by transmission electronic microscopy (TEM), these techniques do not provide fast and clear-cut information regarding their formation and composition. Conversely, electrophoresis relies on a simple and affordable setup and has already been reported as a reliable technique for analyzing and separating NPs of various sizes and shapes[31 32] and as a characterization method for nanomaterials including polymer wrapped inorganic nanoparticles[33] and upconverting nanoparticles.[34] When combined to fluorescence detection, electrophoresis enables highly sensitive detection of fluorescently labeled nanomaterials[35] and nanoconjugates.[36] Consequently, fluorescence labeling of HNPs combined with electrophoresis analysis would enable a precise assessment of their assembly and integrity.

Herein, we fluorescently labeled amphiphilic polymers in red and developed a green emitting fluorogenic oil tracker, thus allowing to independently monitoring the fate and colocalization of the polymer and the oil phase during the formulation of HNPs by nanoprecipitation. Electrophoresis revealed by fluorescence was successfully used as a monitoring method for the formation of HNPs and was found to be a valuable tool providing complementary information compared to DLS and TEM.

[a] *Laboratoire de Bioimagerie et Pathologies, UMR 7021 CNRS, University of Strasbourg, France.*
[b] *Laboratoire de Conception et d'Applications de Biomolécules, UMR 7199 CNRS, University of Strasbourg, France.*

† Footnotes relating to the title and/or authors should appear here.
Electronic Supplementary Information (ESI) available: [details of any supplementary information available should be included here]. See DOI: 10.1039/x0xx00000x

ARTICLE

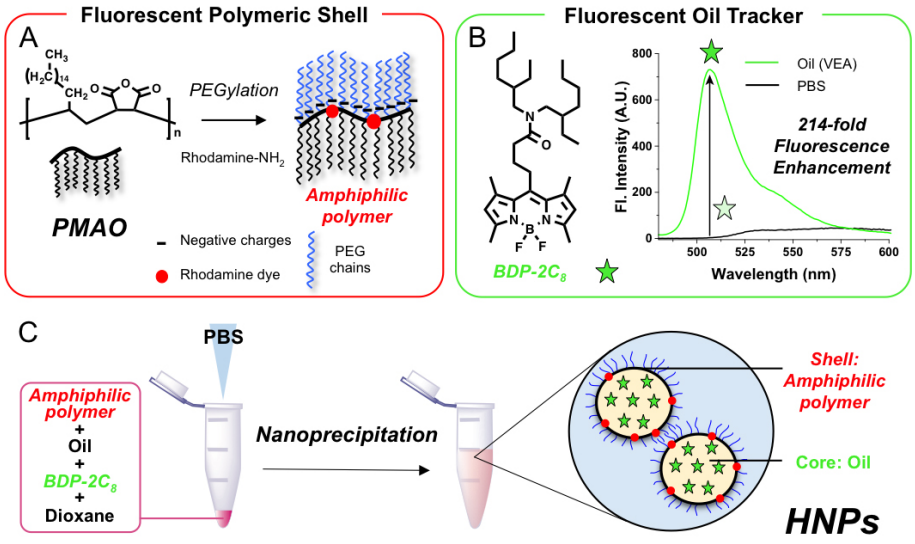

Figure 1. (A) Synthesis of fluorescently labeled amphiphilic polymer. (B) Development of fluorescent oil tracker based on BODIPY BDP-2C_8 and its fluorescent spectra at 1 µM in PBS and in oil. (C) Formulation of HNPs by nanoprecipitation and their schematic representation.

2. Results and discussion

2.1. Fluorescence labeling of HNPs constituents

Herein we aimed at formulating new hybrid nanoparticles (HNPs) based on the wrapping of a lipid droplet by an amphiphilic polymer (Figure 1C) as well as assessing their formation by fluorescence technique using simple methods. Firstly, an amphiphilic polymer was obtained from chemical modification of a commercially available alternating polymer: Poly (maleic anhydride-alt-1-octadecene) (PMAO), which is composed of a repeating unit consisting of a hydrophobic hydrocarbon chain (C16) and an amine reactive succinic anhydride function (Figure 1A). These alternating amphiphilic polymers are widely used to wrap nanocrystals to obtain water soluble inorganic nanoparticles[33] and upconverting nanoparticles.[37] We also showed that PMAO, without any chemical modification, when incorporated at 1 wt % in oil can significantly modify the physicochemical properties of nanoemulsions.[24] PMAO can be readily reacted with Jeffamine, an amine-terminated polypropylene glycol/polyethylene glycol copolymer mainly composed of PEG. Vitamin E acetate (VEA) is a biocompatible and viscous oil that was chosen to constitute the non-polar core of our HNPs as we recently demonstrated its ability to form small and monodisperse fluorescent lipid droplets by spontaneous nanoemulsification.[28] In order to assess the formation of HNPs, both constituents, namely the amphiphilic polymer and the oil, were fluorescently labeled. To this endeavor, 1% of the reactive anhydride sites of PMAO were reacted with Rhodamine–NH_2, a red emitting amino-rhodamine (Figure 1A),[37] while the oil phase was labeled using a newly developed fluorogenic oil tracker consisting of a lipophilic green emitting BODIPY, BDP-2C_8. Indeed, this hydrophobic molecule displayed an impressive fluorescence enhancement at 507 nm from PBS to VEA (214-fold, Figure 1B), and also when incorporated in VEA based nanoemulsions (130-fold, Table S1, Figure S1). Thanks to its hydrophobicity, BDP-2C_8 possesses a high affinity towards lipid oil, as its calculated CLogP was found to be close to the logP of VEA (11.2 and 9.95 respectively). Consequently, two complementary colors channels (green and red) can be used in fluorescence imaging to individually monitor both the oil phase and the polymer during the formulation of HNPs.

Once all the constituents synthesized, two formulation methods were explored. 1) Rehydration of a dry organic film consisting in adding a non-solvent (PBS) on a film containing all the components (Oil/Polymer/BDP-2C_8). 2) A “nanoprecipitation” approach consisting of quickly adding a non-solvent (PBS) to a concentrated solution of the components in dioxane (Figure 1C). While the rehydration approach led to flocculation and heterogeneous solutions, the nanoprecipitation method provided a visually clear nano-suspension and was thus adopted for the rest of our study.

2.2. Formulation & Electrophoresis

In a first experiment, we used the amphiphilic polymer HP1 where all the anhydride functions were reacted with Jeffamine-1000 and 1% with Rhodamine–NH_2 (see SI). This amphiphilic polymer thus displays hydrophobic hydrocarbon chains at one end, PEG chains at the other end and negatively charged carboxylate groups at the interface (Figure 1A). We first assessed the formation of HNPs by varying HP1/oil weight ratio (wt %). To this aim, a solution of VEA (2 mg/mL in dioxane) containing 1 wt % of BDP-2C_8 (as oil tracker) and a solution of HP1 (2 mg/mL in dioxane) were mixed at various ratios, and PBS (95 Vol % of the final volume) was vigorously added for nanoprecipitation at room temperature. The formulations were then first analyzed by DLS. In absence of polymer large and polydisperse (510 ± 307 nm, PDI 0.35) pure oil droplets were obtained (Figure 2 A).

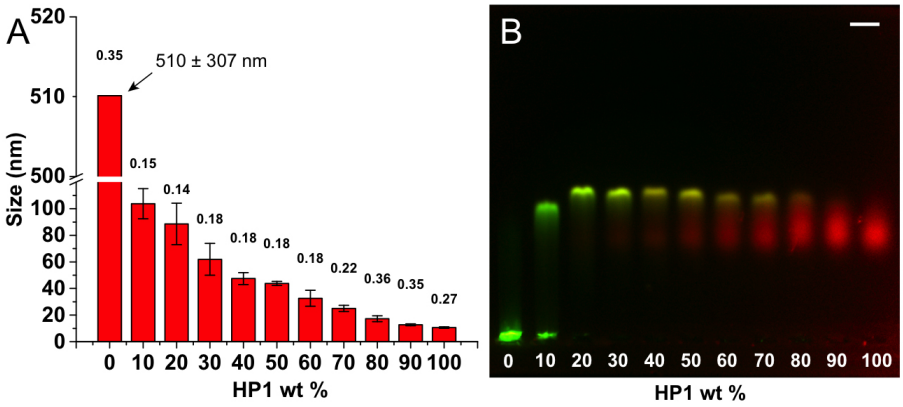

Figure 2. Formulation of HNPs with various polymer/oil wt %. (A) Mean sizes measured by DLS resulting from at least 3 independent formulations. Numbers above the bars are the mean PDI values. (B) Merged green and red channels of the electrophoresis image. Scale bar is 0.5 cm.

Interestingly, at only 10 wt % HP1, dramatic effects were obtained as smaller size (103 ± 11 nm) and improved dispersity (PDI = 0.15) were obtained (Figure 2A). Upon increase of HP1 wt %, the sizes gradually decreased (Figure 2A) to finally reach pure polymer nanoparticles (PPNPs) with size of 10.6 ± 0.6 nm. Although DLS provided information regarding the average size of the bulk formulation, it did not inform on the nature of the formed NPs. In order to provide a deeper characterization of the NPs composition and taking advantage of our fluorescent labels, electrophoresis was performed, allowing for individual tracking of the oil and polymer, using the green and red channels, respectively (Figure 2B). Remarkably, the obtained gel displayed clear-cut and informative results. While in the absence of polymer the oil was unable to migrate to the anode, in the presence of 10 wt % HP1, the green signal was split up in two spots, one corresponding to the initial position (no migration), and the other one to a significant migration of the oil. At 20 wt % HP1, the pure oil spot was undetectable thus showing that this polymer/oil ratio was sufficient to uptake the entire amount of oil into new migrating species. At higher polymer wt %, the red and green fluorescence signals merged perfectly indicating that the new appearing spot might correspond to HNPs composed of both oil and polymer. Interestingly, the use of larger polymer/oil ratios revealed the appearance of a new red fluorescent spot corresponding to pure polymeric NPs (PPNPs). This was confirmed by the formulation in absence of oil that provided a red spot at the same migration distance (Figure 2A, 100 wt % HP1). Compared to DLS, which provides the size distribution of the whole population whatever its composition, this experimental approach appeared much more informative on the composition of the NPs suspension. The electrophoresis clearly discriminated the different populations and revealed the presence of hybrid NPs. According to these first results, 20 wt % polymer was sufficient to formulate HNPs with full uptake of the oil.

In addition to this experiment, another serie of formulations was studied, fixing the amount of oil in order to keep a high green signal and the amount of polymer was gradually increased, ranging from 10 to 50 wt % (results reported in Figure S2). The electrophoresis revealed that, upon an increase of the polymer wt %, the spots corresponding to the HNPs displayed the same yellow color (merge of green and red) with no significant change in their migration distance, whereas the intensity of spots corresponding to PPNPs gradually increased. These results indicated that the formulation of HNPs required a minimum amount of 20 wt % of polymer and that that the additional use of polymer does not lead to its incorporation into HNPs but rather forms a second population of pure polymer nanoparticles (PPNPs).

At that point of our study several controls were performed. First, we checked that the non-migrating and intense green signal obtained in absence of polymer was due BDP-2C_8 dissolved in oil (Figure 3B, formulation 1) and not to BDP-2C_8 itself in aqueous solution. Therefore, BDP-2C_8 was formulated alone in PBS at the same concentration than used in the presence of oil (Figure 3, formulation 2). BDP-2C_8 formulated alone did not provide any signal at the level of pure oil. Instead, a dim orange signal was obtained at a higher migration distance. It is known that pure fluorophores can form aggregates at the nanoscale with low brightness due to Aggregation-Caused Quenching (ACQ).[38, 39] Spectroscopic studies confirmed that BDP-2C_8, when formulated in PBS form dispersed aggregates. First, both absorption and emission spectra dramatically broadened (Figure S1).

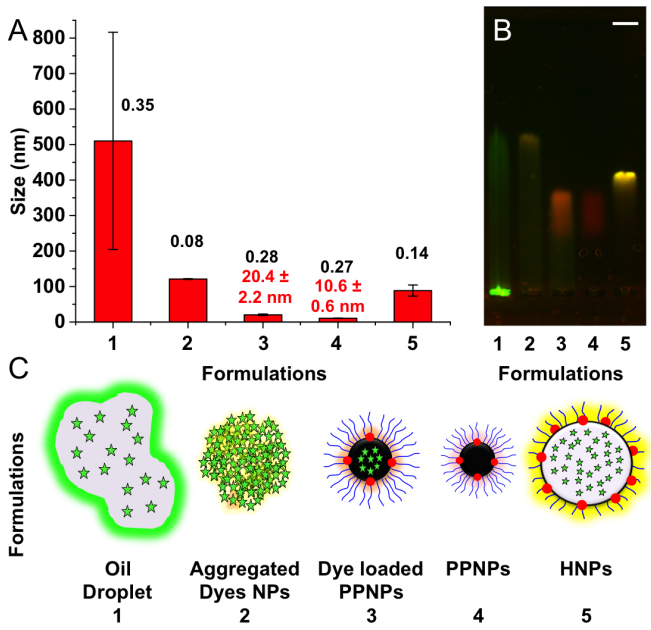

Figure 3. Various formulations studied. (A) Mean sizes measured by DLS resulting from at least 3 independent formulations. (B) Merged green and red channels of the electrophoresis image. Scale bar is 0.5 cm. (C) Schematized structures assigned to the formulations. 1) VEA (100 μg/mL containing) + BDP-2C$_8$ (1 μg/mL); 2) BDP-2C$_8$ (1 μg/mL); 3) HP1 (100 μg/mL) + BDP-2C$_8$ (1 μg/mL); 4) HP1 (100 μg/mL); 5) VEA (80 μg/mL containing) + BDP-2C$_8$ (1 μg/mL) + HP1 (20 μg/mL).

Then, emission spectra also revealed an important red shift. Indeed, while dissolved in oil BDP-2C$_8$ emitted at 500 nm with high quantum yield (0.82), pure BDP-2C$_8$ NPs emitted at 577 nm with a notable quantum yield of 0.19 (table S1), explaining the dim orange spot obtained in electrophoresis (Figure 3B, formulation 2).

This phenomenon was already reported for BODIPY fluorophores and was attributed to the formation of red shifted emissive *J*-Aggregates.[40] In addition, DLS measurements corroborated that BDP-2C$_8$, when formulated in PBS, aggregated as monodisperse NPs (121 ± 1 nm, PDI = 0.08, Figure 3A formulation 2). This experiment confirmed that the non-migrating green spot resulted from the oil droplets containing BDP-2C$_8$. Then, the polymer (HP1) was formulated in the presence of BDP-2C$_8$ and in the absence of oil (formulation 3) in order to verify whether the spots correspond to PPNs or overlap with HNPs (Figure 3, formulation 4 and 5, respectively). This control experiment showed that the migration spot of pure BDP-2C$_8$ NPs (formulation 2) disappeared, giving rise to an orange signal (formulation 3) that appeared at the same level than PPNPs (formulation 4), with similar small sizes (20 ± 2 nm and 11 ± 1 nm for formulations 3 and 4, respectively). This experiment showed the ability of PPNPs to efficiently entrap BDP-2C$_8$ providing a different spot than HNPs. Overall, these controls proved that an intense green signal is obtained only in the presence of the oil, and thus, that the colocalization of green and red signals (*i.e.* intense yellow spot), was correctly assigned to HNPs (Figure 3, formulation 5).

Since electrophoresis was used to monitor and optimize the formation of HNPs, we hypothesized that it could also serve to assess their stability. To this end, HNPs composed of HP1 (20 wt %) were formulated and submitted to a temperature of 60°C over 4h. Every 30 min the size was measured by DLS and a small aliquot was kept for electrophoresis (Figure S3). On the one hand, we can note that although the size and the PDI only slightly increased over the time, the electrophoresis showed clear signs of degradation. Then, the migration distance of the spot corresponding to HNPs slightly decreased over the time along with its red color probably denoting a partial erosion of the polymer leading to the destabilization of the HNPs. At last, the green spots located at the deposition well, corresponding to pure oil, gradually appeared over the time. Overall, the electrophoresis clearly depicted a phase separation between the oil and the polymer over the time at 60°C and thus appeared as an efficient method to assess the stability of the fluorescently labeled HNPs.

2.3. Transmission Electronic Microscopy (TEM)

According to the obtained results, electrophoresis when correlated to DLS, provided evidences that HNPs can be obtained by simple nanoprecipitation using PMAO based amphiphilic polymer HP1. As complementary studies, HNPs composed of HP1 (20 wt %) were characterized by TEM.

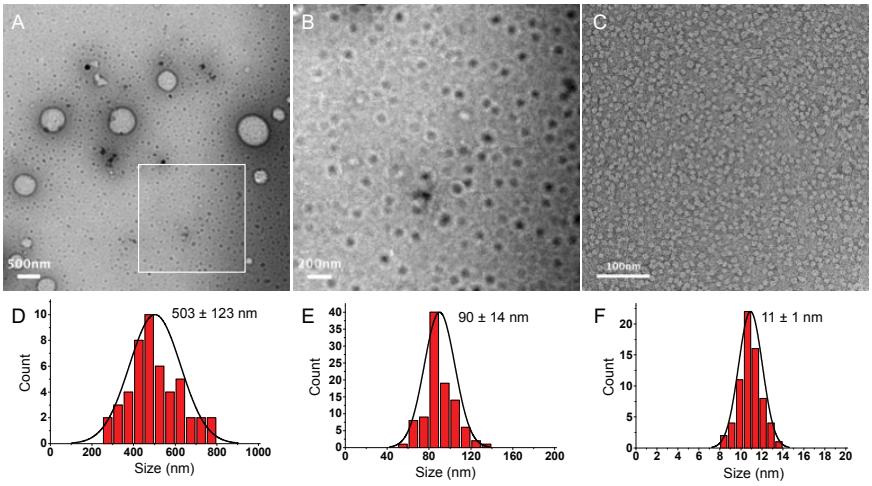

Figure 4. (A) TEM image of HNPs composed of HP1 (20 wt %). (B) is the zoomed region of interest in (A). (C) TEM image of PPNPs composed of HP1. D, E and F are the corresponding histograms of the measured particles' sizes.

The images revealed the presence of 2 populations of particles (Figure 4A). The first population, present at a lower extent, displayed a spherical shape with a mean size of 503 ± 123 nm combined with a large polydispersity (Figure 4D). This was in accordance with the DLS measurements of pure VEA droplets (Figure 3A, formulation 1), probably resulting from the phase separation between oil and polymer during the preparation of the TEM sample at high vacuum. This type of images were already observed in TEM with nano-emulsions containing vitamin E-based compounds (or oils of similar viscosity), giving rise to spherical droplets that spread onto the carbon support.[41, 42] The second population, present at a higher extent, displayed spherical shapes (Figure 4B) with an average size of 90 ± 14 nm (Figure 4E) and was attributed to HNPs; as their size was similar to the DLS measurements (Figure 3A, formulation 5). As a control, formulation involving only HP1 in absence of oil was imaged. TEM images revealed that PPNPs formed a dense layer of spread particles (Figure 4C) with an average size of 11 ± 1 nm (Figure 4F), which was again in accordance with DLS (Figure 3A, formulation 4).

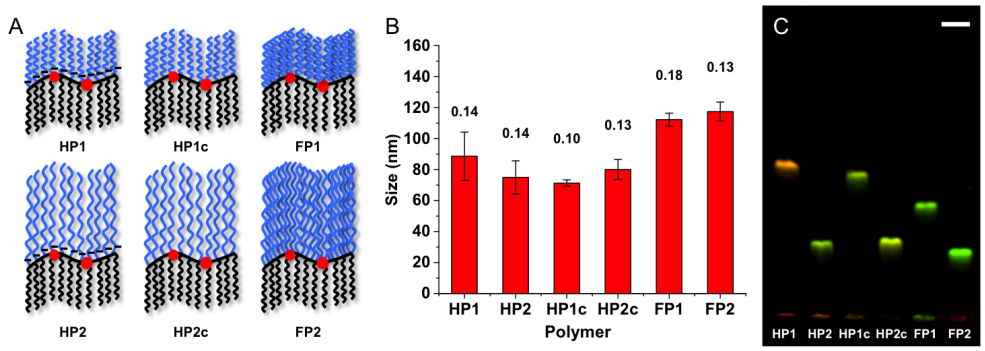

Figure 5. Formulation of 20 wt % polymer HNPs with different amphiphilic polymers. (A) Schematic representation of the polymers used for formulation. (B) Mean sizes measured by DLS resulting from at least 3 independent formulations. Numbers above the bars are the mean PDI values. (C) Merged green and red channels of the electrophoresis image. Scale bar is 0.5 cm.

2.4. Use of various amphiphilic polymers

We showed that fluorescent labeling of oil and polymer in combination with electrophoresis analysis could be used to monitor the formation and degradation of HNPs. We then chemically modified the amphiphilic nature of PMAO-based polymers to assess their ability to form HNPs and use this new experimental approach to disclose the impact of their chemical structure on the formulations. To this end, various PMAO-based amphiphilic polymers were synthesized (Figure 5A). Jeffamine-1000 and Jeffamine-2000 were used to modulate the PEG length and thus gave rise to HP1, HP1c, FP1 and HP2, HP2c and FP2 respectively. The negative charges brought by the remaining carboxylates groups (COO^-) were capped either by coupling with an excess of short ethanolamine molecules to give HP1c, HP2c, or by coupling supplementary Jeffamine PEG chains giving rise to fully PEGylated polymers, FP1 and FP2. Accordingly to our previous results, the formulations were performed with 20 wt % amphiphilic polymers and 80 wt % VEA in PBS. These formulations were analyzed by DLS (Figure 5B) and by electrophoresis (Figure 5C). First, the electrophoresis showed that all of the polymers when used at 20 wt %, were able to form HNPs. The obtained sizes by DLS spanned within a small range, from 71 ± 2 nm (HP1c) to 117 ± 6 nm (FP2) with larger sizes obtained with the fully PEGylated polymers. The slight difference in DLS size might be explained by the difference of molecular weight especially between the half PEGylated and the fully PEGylated polymers. Indeed although the wt % was kept at 20%, the molar polymer/oil ratio is significantly smaller in the case of "heavy" polymers that led to larger HNPs, this is consistent with our previous observation (figure2A). Additionally, while full PEGylation led to slightly lower migration distances compared to half PEGylation, the use of large PEG-2000 systematically led to an important decrease of migration. It is noteworthy that charge capping by ethanolamine, while slightly enhanced the monodispersity of the obtained HNPs compared to the charged polymers, hardly influenced their migration distance and their size. Although the efficiency of the chemical reactions performed on the polymer was confirmed by ^{1}H NMR (see SI), the measured ζ potential displayed similar values (~26 mV, Table S2). The correlation between electrophoretic migration and values of ζ potential from charged and capped polymers suggests that the particles still present a significant surface potential, which can come from various origins, PEG chain conformations, dipoles and interactions of the ions present in the media. Overall, it appeared that the nature of the amphiphilic polymer, more precisely its PEGylation rate, but also the length of the PEG

chains significantly influenced the migration distance of the HNPs. To further support this hypothesis, a fully ethanolamine-capped polymer was used to study the influence of PEG groups on the formulation of HNPs (Figure S4). Interestingly the electrophoresis showed that neither the polymer nor the oil migrated indicating that this less polar polymer failed to form HNPs at any polymer/oil ratio. These results underline the major role of PEG chains in the formulation of HNPs. Eventually, the electrophoresis appeared to be a method of choice also adapted to characterize the surface modifications of these HNPs.

3. Conclusion

Herein, we aimed at developing new lipid-core/polymer-shell hybrid nanoparticles (HNPs) by simple nanoprecipitation protocol. In order to facilitate the screening of the optimal conditions, both oil and polymer constituents were fluorescently labeled with distinct colors. To this end, the amphiphilic polymer was covalently labeled with a red emitting rhodamine and in parallel, an oil tracker was developed based on a hydrophobic fluorogenic BODIPY displaying a 214-fold fluorescence enhancement from PBS to oil. The obtained formulations were systematically analyzed by DLS and through an innovative experimental approach using dual color fluorescently revealed electrophoresis. We herein showed that, unlike DLS measurements and TEM imaging, electrophoresis provides unambiguous information by discrimination of the different nanomaterials that can be obtained during the formulation. Additionally, we showed that this technique could be used to assess the stability of the lipid nanomaterial, as well as to discriminate the relationships between particle composition and surface properties. We believe that, in the future, this method might facilitate the development of new lipid nanoparticles by accelerating the optimization of the formulation conditions. Finally, the herein presented hybrid nanomaterials present many advantages in terms of preparation and chemical modifications. Consequently, ongoing work is being performed by our group to develop functionnalizable hybrid particles based on this approach.

4. Experimental section

4.1. Materials

Poly (maleic anhydride-alt-1-octadecene) (PMAO, Average Mn 30,000-50,000), diisopropylethyl amine (DIEA), ethanolamine, tetrahydrofuran (THF) and dioxane were purchased from Sigma Aldrich. Jeffamine M-1000 (J-1000) and Jeffamine M-2070 (J-2000) polyetheramine (J-2000) were kindly offered by Huntsman Corporation (Texas, U.S.A.). Vitamin E acetate (VEA) was purchased form TCI Europe. The solvents were of analytical grade, Dimethylformamide (DMF) was anhydrous.

4.2 Synthesis

NMR spectra were recorded on a Bruker Avance III 400 MHz spectrometer. Mass spectra were obtained using an Agilent Q-TOF 6520 mass spectrometer. Spectra can be found in the supplementary information. cLogP value of BDP-2C_8 was obtained using ChemDraw (Cambridge software).

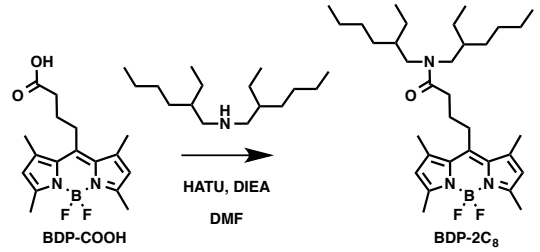

BDP-2C_8. To a solution of acid BDP-COOH (200 mg, 0.598 mmol, 1 eq) in DMF (4 mL) under Argon, was added bis(2-ethylhexyl)amine (0.270 mL, 0.897 mmol, 1.5 eq), followed by DIEA (0.313 mL, 1.790 mmol, 3 eq) and HATU (273 mg, 0.718 mmol, 1 .2 eq). The reaction mixture was allowed to stir for 1h. The excess of solvent was evaporated. The crude was extracted with DCM and washed with water (x2) and brine (x2). The organic phase was dried over anhydrous $MgSO_4$, filtered and evaporated. The product was purified by chromatography column on silica gel using DCM/EtOAc (98/2). 159 mg of BDP-2C_8 was obtained (Yield= 48%) as an orange powder. Rf= 0.25 (100% DCM). ^{1}H-NMR (400 MHz, $CDCl_3$): δ 6.07 (s, 2H, H), 3.29 (ddd, *J* = 14.0, 7.4, 1.6 Hz, 2H, 2 N-CH), 3.15 (d, *J* = 7.5 Hz, 2H, 2 N-CH), 3.05-3.01 (m, 2H, CH_2), 2.53-2.47 (m, 14H, 4 CH_3, CH_2), 2.05-1.97 (m, 2H, CH_2), 1.67 (s, 1H, CH), 1.60 (s, 1H, CH), 1.36-1.19 (m, 16H, 8 CH_2), 0.94-0.86 (m, 12H, 4 CH_3). ^{13}C-NMR (101 MHz, $CDCl_3$): δ 171.9, 153.9, 145.7, 140.5, 131.5, 131.5, 121.6, 51.5, 48.9, 38.6, 37.0, 33.0, 30.6, 30.5, 28.8, 28.7, 28.7, 27.7, 27.4, 23.9, 23.8, 23.0, 23.0, 16.4, 14.4, 14.4, 14.4, 14.0, 14.0, 10.8, 10.6, 10.6. HRMS (ESI$^+$), calculated for $C_{33}H_{54}BF_2N_3ONa$ $[M+Na]^+$: 580.4426, found 580.4213. Calculated for $C_{33}H_{54}BFN_3O$ $[M-F]^+$: 538.4344, found 538.4329. Calculated for $C_{33}H_{54}BF_2N_3ONa$ $[2M+Na]^+$: 1137.8554, found 1137.8528.

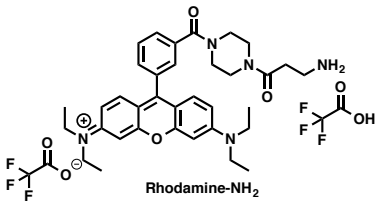

Rhodamien-NH_2. We described the synthesis of rhodamine-NH_2 elsewhere.[43]

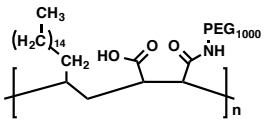

HP1. To a solution of PMAO (30 mg, 85.71 μmol of repeating unit see SI) in degassed anhydrous DMF (3 mL) was added a solution of a Rhodamine-NH_2 (8.57 mol, 69 μL C=10 mg/mL in DMF) followed by DIEA (0.85 mmol, 200 mL, 10 eq) and a

solution of Jeffamine-1000 (1 mL, C=100 mg/mL in DMF, 0.102 mmol, 1.2 eq). The reaction mixture was allowed to stir for 2 h before the addition of few drops of water. The solvents were evaporated. The crude was purified by size exclusion column using DCM/MeOH (1/1). 61 mg of HP1 was obtained as a pink sirup (Yield= 53%).
The synthesis of the other polymers can be found in the supplementary information.

4.3 Spectroscopy.

For spectroscopy the concentration of BDP-2C_8 was 1 μM and solvents were of spectroscopic grade. The water was milliQ water. Absorption and emission spectra were recorded on a Cary 400 Scan ultraviolet–visible spectrophotometer (Varian) and a FluoroMax-4 spectrofluorometer (Horiba Jobin Yvon) equipped with a thermostated cell compartment, respectively. For standard recording of fluorescence spectra, the emission was collected 10 nm after the excitation wavelength. All the spectra were corrected from wavelength-dependent response of the detector. The quantum yields were determined by comparison with fluorescein[44] (in NaOH 0.1 M, ϕ= 0.95) following equation (1):

$$\mathrm{QY} = \mathrm{QY}_R \times \frac{I \times OD_R \times n^2}{I_R \times OD \times n_R^2}$$

Where QY is the quantum yield, I is the integrated fluorescence intensity, n is the refractive index, and OD is the optical density at the excitation wavelength. R represents the reference.

4.4. Formulation of the HNPs

Preparation of stock solutions: First, the oil (VEA) was labeled by dissolving BDP-2C_8 at 1 wt %. The labeled oil was then dissolved in dioxane to reach a concentration of 2 mg/mL. Polymers were dissolved in dioxane at a concentration of 2 mg/mL. The HNPs were formulated using two different methods: 1) Rehydration of films: In a round-bottom flask of 10 mL, 50 μL of premixed solutions of polymer and oil (according to the chosen ratio) were added before being slowly evaporated until obtaining a thin film. Then, 950 μL of PBS were vigorously added using back and forth pipetting using a 1 mL micropipette. 2) Nanoprecipitation: In an Eppendorf tube, stock solutions of polymer and oil (according to the chosen ratio) were added and mixed to reach a final volume of 50 μL. Then, 950 μL of PBS were vigorously added using back and forth pipetting using a 1 mL micropipette. The solution was immediately vortexed for 10 seconds.

4.5. Dynamic Light Scattering (DLS), and ζ potential

After the formulation, size of HPNs were measured by Dynamic Light Scattering with the instrument Zetasizer® Nano ZSP (Malvern, UK) using the formulation solutions. Measurements were performed at 25°C. Refractive index were set to 1.33 for the continuous phase (water) and 1.49 for the dispersed phase (Vitamin E Acetate). Both size distribution and polydispersity index (PDI) were recorded. The ζ potentials were measured on diluted solution in distilled water (0.02 μg/mL) at a stable conductivity of 0.05 mS/cm.

4.6. Electrophoresis

Gel electrophoresis was prepared by dissolving agarose (0.5 wt %) in TAE (Tris Acetate 40 mM, EDTA 1 mM). 13 μL of the formulation solutions were carefully added in the wells. The electrophoresis was run at 125 V for 1h. The gels were visualized with an ImageQuant LAS 4000 (GE Healthcare Life Sciences) using Cy2 (excitation: 473 nm) and Cy3 (excitation: 532 nm) channels and by acquiring successive images with an exposition time of 10 seconds. The images were treated with ImageJ.

4.7 Stability assay

HNPs composed of HP1 (20 wt %) were formulated as described in 4.4 and placed in a 1.6 mL cuvette for DLS measurement. The cuvette was then closed by help of an adapted stopper and was warmed at 60°C in a water bath. At each time point, the solution was rapidly cooled down to RT; then a DLS measurement was performed and 30 μL was taken off for electrophoresis.

4.8. Transmission Electron Microscopy (TEM)

5 μL of the formulation solution was deposited onto carbon-coated copper-rhodium electron microscopy grids that were used following amylamine glow-discharge. The grids were then treated for 1 min with a 2 % uranyl acetate solution for staining and observed with a Philips CM120 transmission electron microscope equipped with a LaB_6 filament and operating at 100 kV. Areas covered with NPs of interest were recorded on a Peltier cooled CCD camera (Model 794, Gatan, Pleasanton, CA). Image analysis was performed using the imageJ software.

Conflicts of interest

The authors declare no conflict of interest.

Acknowledgements

This work was supported by the European Research Council (ERC) Consolidator grant BrightSens 648528 and the French National Research Agency (ANR) BrightRiboProbes (ANR-16-CE11-0010). XW was founded by the China Scholarship Council PhD fellowship (CSC No. 201706240033). The authors would like to thank Dr. Delphine Garnier from the Analytical platform (PACSI) for her assistance in the LC-MS and RMN analyses. We also thank Huntsman Corporation for providing Jeffamine-M-1000 and Jeffamine-M-2070.

Notes and references

1 (1) Mandal, B.; Bhattacharjee, H.; Mittal, N.; Sah, H.; Balabathula, P.; Thoma, L. A.; Wood, G. C. Core–shell-Type Lipid–polymer Hybrid Nanoparticles as a Drug Delivery Platform. *Nanomedicine Nanotechnol. Biol. Med.* **2013**, *9* (4), 474–491. https://doi.org/10.1016/j.nano.2012.11.010.

2 (2) Khan, A. A.; Mudassir, J.; Mohtar, N.; Darwis, Y. Advanced Drug Delivery to the Lymphatic System: Lipid-Based Nanoformulations. *Int. J. Nanomedicine* **2013**, *8*, 2733. https://doi.org/10.2147/IJN.S41521.

3 (3) Anton, N.; Vandamme, T. F. The Universality of Low-Energy Nano-Emulsification. *Int. J. Pharm.* **2009**, *377* (1–2), 142–147. https://doi.org/10.1016/j.ijpharm.2009.05.014.

4 (4) McClements, D. J. Nanoemulsions versus Microemulsions: Terminology, Differences, and Similarities. *Soft Matter* **2012**, *8* (6), 1719–1729. https://doi.org/10.1039/C2SM06903B.

5 (5) Yao, M.; Xiao, H.; McClements, D. J. Delivery of Lipophilic Bioactives: Assembly, Disassembly, and Reassembly of Lipid Nanoparticles. *Annu. Rev. Food Sci. Technol.* **2014**, *5*, 53–81. https://doi.org/10.1146/annurev-food-072913-100350.

6 (6) Mehnert, W.; Mäder, K. Solid Lipid Nanoparticles: Production, Characterization and Applications. *Adv. Drug Deliv. Rev.* **2001**, *47* (2–3), 165–196.

7 (7) Naseri, N.; Valizadeh, H.; Zakeri-Milani, P. Solid Lipid Nanoparticles and Nanostructured Lipid Carriers: Structure, Preparation and Application. *Adv. Pharm. Bull.* **2015**, *5* (3), 305. https://doi.org/10.15171/apb.2015.043.

8 (8) Mukherjee, S.; Ray, S.; Thakur, R. S. Solid Lipid Nanoparticles: A Modern Formulation Approach in Drug Delivery System. *Indian J. Pharm. Sci.* **2009**, *71* (4), 349. https://doi.org/10.4103/0250-474X.57282.

9 (9) Li, Q.; Cai, T.; Huang, Y.; Xia, X.; Cole, S. P. C.; Cai, Y. A Review of the Structure, Preparation, and Application of NLCs, PNPs, and PLNs. *Nanomater. Basel Switz.* **2017**, *7* (6). https://doi.org/10.3390/nano7060122.

10 (10) Iqbal, M. A.; Md, S.; Sahni, J. K.; Baboota, S.; Dang, S.; Ali, J. Nanostructured Lipid Carriers System: Recent Advances in Drug Delivery. *J. Drug Target.* **2012**, *20* (10), 813–830. https://doi.org/10.3109/1061186X.2012.716845.

11 (11) Li, X.; Anton, N.; Zuber, G.; Zhao, M.; Messaddeq, N.; Hallouard, F.; Fessi, H.; Vandamme, T. F. Iodinated α-Tocopherol Nano-Emulsions as Non-Toxic Contrast Agents for Preclinical X-Ray Imaging. *Biomaterials* **2013**, *34* (2), 481–491. https://doi.org/10.1016/j.biomaterials.2012.09.026.

12 (12) Attia, M. F.; Anton, N.; Chiper, M.; Akasov, R.; Anton, H.; Messaddeq, N.; Fournel, S.; Klymchenko, A. S.; Mély, Y.; Vandamme, T. F. Biodistribution of X-Ray Iodinated Contrast Agent in Nano-Emulsions Is Controlled by the Chemical Nature of the Oily Core. *ACS Nano* **2014**, *8* (10), 10537–10550. https://doi.org/10.1021/nn503973z.

13 (13) Kumari, A.; Yadav, S. K.; Yadav, S. C. Biodegradable Polymeric Nanoparticles Based Drug Delivery Systems. *Colloids Surf. B Biointerfaces* **2010**, *75* (1), 1–18. https://doi.org/10.1016/j.colsurfb.2009.09.001.

14 (14) Elsabahy, M.; Wooley, K. L. Design of Polymeric Nanoparticles for Biomedical Delivery Applications. *Chem. Soc. Rev.* **2012**, *41* (7), 2545–2561. https://doi.org/10.1039/c2cs15327k.

15 (15) Delplace, V.; Couvreur, P.; Nicolas, J. Recent Trends in the Design of Anticancer Polymer Prodrug Nanocarriers. *Polym. Chem.* **2014**, *5* (5), 1529–1544. https://doi.org/10.1039/C3PY01384G.

16 (16) Reisch, A.; Klymchenko, A. S. Fluorescent Polymer Nanoparticles Based on Dyes: Seeking Brighter Tools for Bioimaging. *Small Weinh. Bergstr. Ger.* **2016**, *12* (15), 1968–1992. https://doi.org/10.1002/smll.201503396.

17 (17) Kamaly, N.; Yameen, B.; Wu, J.; Farokhzad, O. C. Degradable Controlled-Release Polymers and Polymeric Nanoparticles: Mechanisms of Controlling Drug Release. *Chem. Rev.* **2016**, *116* (4), 2602–2663. https://doi.org/10.1021/acs.chemrev.5b00346.

18 (18) Raemdonck, K.; Braeckmans, K.; Demeester, J.; Smedt, S. C. D. Merging the Best of Both Worlds: Hybrid Lipid-Enveloped Matrix Nanocomposites in Drug Delivery. *Chem. Soc. Rev.* **2013**, *43* (1), 444–472. https://doi.org/10.1039/C3CS60299K.

19 (19) Zhang, R. X.; Ahmed, T.; Li, L. Y.; Li, J.; Abbasi, A. Z.; Wu, X. Y. Design of Nanocarriers for Nanoscale Drug Delivery to Enhance Cancer Treatment Using Hybrid Polymer and Lipid Building Blocks. *Nanoscale* **2017**, *9* (4), 1334–1355. https://doi.org/10.1039/C6NR08486A.

20 (20) Hadinoto, K.; Sundaresan, A.; Cheow, W. S. Lipid–polymer Hybrid Nanoparticles as a New Generation Therapeutic Delivery Platform: A Review. *Eur. J. Pharm. Biopharm.* **2013**, *85* (3, Part A), 427–443. https://doi.org/10.1016/j.ejpb.2013.07.002.

21 (21) Dave, V.; Tak, K.; Sohgaura, A.; Gupta, A.; Sadhu, V.; Reddy, K. R. Lipid-Polymer Hybrid Nanoparticles: Synthesis Strategies and Biomedical Applications. *J. Microbiol. Methods* **2019**, *160*, 130–142. https://doi.org/10.1016/j.mimet.2019.03.017.

22 (22) Zhang, L.; Zhang, L. Lipid–polymer Hybrid Nanoparticles: Synthesis, Characterization and Applications. *Nano LIFE* **2010**, *01* (01n02), 163–173. https://doi.org/10.1142/S179398441000016X.

23 (23) Oh, K. S.; Lee, K. E.; Han, S. S.; Cho, S. H.; Kim, D.; Yuk, S. H. Formation of Core/Shell Nanoparticles with a Lipid Core and Their Application as a Drug Delivery System. *Biomacromolecules* **2005**, *6* (2), 1062–1067. https://doi.org/10.1021/bm049234r.

24 (24) Attia, M. F.; Dieng, S. M.; Collot, M.; Klymchenko, A. S.; Bouillot, C.; Serra, C. A.; Schmutz, M.; Er-Rafik, M.; Vandamme, T. F.; Anton, N. Functionalizing Nanoemulsions with Carboxylates: Impact on the Biodistribution and Pharmacokinetics in Mice. *Macromol. Biosci.* **2017**, *17* (7), 1600471. https://doi.org/10.1002/mabi.201600471.

25 (25) Lipid Nanocapsules: A New Platform for Nanomedicine. *Int. J. Pharm.* **2009**, *379* (2), 201–209. https://doi.org/10.1016/j.ijpharm.2009.04.026.

26 (26) Texier, I.; Goutayer, M.; Da Silva, A.; Guyon, L.; Djaker, N.; Josserand, V.; Neumann, E.; Bibette, J.; Vinet, F. Cyanine-Loaded Lipid Nanoparticles for Improved in Vivo Fluorescence Imaging. *J. Biomed. Opt.* **2009**, *14* (5), 054005-054005-11. https://doi.org/10.1117/1.3213606.

27 (27) Bouchaala, R.; Mercier, L.; Andreiuk, B.; Mély, Y.; Vandamme, T.; Anton, N.; Goetz, J. G.; Klymchenko, A. S. Integrity of Lipid Nanocarriers in Bloodstream and Tumor Quantified by Near-Infrared Ratiometric FRET Imaging in Living Mice. *J. Controlled Release* **2016**, *236*, 57–67. https://doi.org/10.1016/j.jconrel.2016.06.027.

28 (28) WANG, X.; Anton, N.; Ashokkumar, P.; Anton, H.; Fam, T. K.; Vandamme, T. F.; Klymchenko, A. S.; Collot, M. Optimizing the Fluorescent Properties of Nano-Emulsions for Single Particle Tracking in Live Cells. *ACS Appl. Mater. Interfaces* **2019**. https://doi.org/10.1021/acsami.8b22297.

29 (29) Kilin, V. N.; Anton, H.; Anton, N.; Steed, E.; Vermot, J.; Vandamme, T. F.; Mely, Y.; Klymchenko, A. S. Counterion-Enhanced Cyanine Dye Loading into Lipid Nano-Droplets for Single-Particle Tracking in Zebrafish. *Biomaterials* **2014**, *35* (18), 4950–4957. https://doi.org/10.1016/j.biomaterials.2014.02.053.

30 (30) Klymchenko, A. S.; Roger, E.; Anton, N.; Anton, H.; Shulov, I.; Vermot, J.; Mely, Y.; Vandamme, T. F. Highly Lipophilic Fluorescent Dyes in Nano-Emulsions: Towards Bright Non-Leaking Nano-Droplets. *RSC Adv.* **2012**, *2* (31), 11876–11886. https://doi.org/10.1039/C2RA21544F.

31 (31) Hanauer, M.; Pierrat, S.; Zins, I.; Lotz, A.; Sönnichsen, C. Separation of Nanoparticles by Gel Electrophoresis According to Size and Shape. *Nano Lett.* **2007**, *7* (9), 2881–2885. https://doi.org/10.1021/nl071615y.

32 (32) López-Lorente, A. I.; Simonet, B. M.; Valcárcel, M. Electrophoretic Methods for the Analysis of Nanoparticles. *TrAC Trends Anal. Chem.* **2011**, *30* (1), 58–71. https://doi.org/10.1016/j.trac.2010.10.006.

33 (33) Quarta, A.; Curcio, A.; Kakwere, H.; Pellegrino, T. Polymer Coated Inorganic Nanoparticles: Tailoring the Nanocrystal Surface for Designing Nanoprobes with Biological Implications. *Nanoscale* **2012**, *4* (11), 3319–3334. https://doi.org/10.1039/C2NR30271C.

34 (34) Hlaváček, A.; Sedlmeier, A.; Skládal, P.; Gorris, H. H. Electrophoretic Characterization and Purification of Silica-Coated Photon-Upconverting Nanoparticles and Their Bioconjugates. *ACS Appl. Mater. Interfaces* **2014**, *6* (9), 6930–6935. https://doi.org/10.1021/am500732y.

35 (35) Fernández-Argüelles, M. T.; Yakovlev, A.; Sperling, R. A.; Luccardini, C.; Gaillard, S.; Sanz Medel, A.; Mallet, J.-M.; Brochon, J.-C.; Feltz, A.; Oheim, M.; et al. Synthesis and Characterization of Polymer-Coated Quantum Dots with Integrated Acceptor Dyes as FRET-Based Nanoprobes. *Nano Lett.* **2007**, *7* (9), 2613–2617. https://doi.org/10.1021/nl070971d.

36 (36) Pellegrino, T.; Sperling, R. A.; Alivisatos, A. P.; Parak, W. J. Gel Electrophoresis of Gold-DNA Nanoconjugates. *J. Biomed. Biotechnol.* **2007**, *2007*. https://doi.org/10.1155/2007/26796.

37 (37) Dukhno, O.; Przybilla, F.; Collot, M.; Klymchenko, A.; Pivovarenko, V.; Buchner, M.; Muhr, V.; Hirsch, T.; Mély, Y. Quantitative Assessment of Energy Transfer in Upconverting Nanoparticles Grafted with Organic Dyes. *Nanoscale* **2017**, *9* (33), 11994–12004. https://doi.org/10.1039/C6NR09706E.

38 (38) Shulov, I.; Oncul, S.; Reisch, A.; Arntz, Y.; Collot, M.; Mely, Y.; Klymchenko, A. S. Fluorinated Counterion-Enhanced Emission of Rhodamine Aggregates: Ultrabright Nanoparticles for Bioimaging and Light-Harvesting. *Nanoscale* **2015**, *7* (43), 18198–18210. https://doi.org/10.1039/c5nr04955e.

39 (39) Trofymchuk, K.; Valanciunaite, J.; Andreiuk, B.; Reisch, A.; Collot, M.; Klymchenko, A. S. BODIPY-Loaded Polymer Nanoparticles: Chemical Structure of Cargo Defines Leakage from Nanocarrier in Living Cells. *J. Mater. Chem. B* **2019**, *7* (34), 5199–5210. https://doi.org/10.1039/C8TB02781A.

40 (40) Choi, S.; Bouffard, J.; Kim, Y. Aggregation-Induced Emission Enhancement of a Meso-Trifluoromethyl BODIPY via J-Aggregation. *Chem. Sci.* **2013**, *5* (2), 751–755. https://doi.org/10.1039/C3SC52495G.

41 (41) Li, X.; Anton, N.; Zuber, G.; Zhao, M.; Messaddeq, N.; Hallouard, F.; Fessi, H.; Vandamme, T. F. Iodinated α-Tocopherol Nano-Emulsions as Non-Toxic Contrast Agents for Preclinical X-Ray Imaging. *Biomaterials* **2013**, *34* (2), 481–491. https://doi.org/10.1016/j.biomaterials.2012.09.026.

42 (42) Attia, M. F.; Anton, N.; Chiper, M.; Akasov, R.; Anton, H.; Messaddeq, N.; Fournel, S.; Klymchenko, A. S.; Mély, Y.; Vandamme, T. F. Biodistribution of X-Ray Iodinated Contrast Agent in Nano-Emulsions Is Controlled by the Chemical Nature of the Oily Core. *ACS Nano* **2014**, *8* (10), 10537–10550. https://doi.org/10.1021/nn503973z.

43 (43) Dukhno, F. Przybilla, M. Collot, A. Klymchenko, V. Pivovarenko, M. Buchner, V. Muhr, T. Hirsch and Y. Mély, *Nanoscale*, 2017, **9**, 11994–12004.

44 (44) Lakowicz, J. R. *Principles of Fluorescence Spectroscopy*; Springer Science & Business Media, 2007.

Graphical abstract